Table VII. Comparison of Force Constants from the Pseudo-Diatomic Model, k_s (P.D.), from a Two-Component Force Field Model, k_s (F.F.); Well Depths, ϵ, and Bending Force Constants, k_θ, for Argon-Furan and Related Complexes

	k_s (P.D.), mdyn/Å	ϵ, cm^{-1}	k_s (F.F.), mdyn/Å	k_θ, mdyn/Å	bond length, Å
argon-furan	0.0269	236	0.0272	0.0354	3.54
argon-ClCN[a]		172	0.0185	0.0333	3.65
argon-BF_3[b]	0.0211	163			3.33
argon-CO_2[c]		148	0.0174	0.0165	3.49
argon-HCl[d,e]	0.0117	128	0.0164	0.0015	
argon-HBr[d]	0.0076	89	0.0166	0.0014	

[a] See ref 3; ϵ calculated from data in ref 3. [b] Values calculated using data in ref 15. [c] See ref 5; ϵ from data in ref 5. [d] See M. R. Keenan, E. J. Campbell, T. J. Balle, L. W. Buxton, T. K. Minton, P. D. Soper, and W. H. Flygare, *J. Chem. Phys.*, 72, 3070 (1980). [e] See M. R. Keenan, L. W. Buxton, E. J. Campbell, T. J. Balle, and W. H. Flygare, *J. Chem. Phys.*, 73, 3523 (1980).

Table VIII. Derivatives of Rotational Constants for Argon-Furan with Respect to Changes in R_0 and θ

$\partial A/\partial R_0 = 12.64$ MHz/Å	$\partial A/\partial\theta = 1133$ MHz
$\partial B/\partial R_0 = 656.2$ MHz/Å	$\partial B/\partial\theta = 87.4$ MHz
$\partial C/\partial R_0 = 651.5$ MHz/Å	$\partial C/\partial\theta = 90.8$ MHz

note that the bending constant k_θ is similar to that obtained for Ar-ClCN.

The τ centrifugal distortion constants may also be used to obtain information on the force constants holding the complex together. We consider a simple force field represented by k_s and k_θ where k_s is associated with changes in the bond length R_0 and k_θ with changes in θ. There will also be a force constant for motion of the argon in the direction of the b axis of the complex but since first derivatives of moments of inertia with respect to this coordinate vanish, it will not contribute to the τ's. We will neglect τ's of the form $\tau_{\alpha\beta\alpha\beta}$ with $\alpha \neq \beta$. In this case we can write

$$\tau_{\alpha\alpha\beta\beta} = -2h\sum_i \frac{\partial G_\alpha}{\partial R_i}\frac{\partial G_\beta}{\partial R_i}\left(\frac{1}{k_i}\right)$$

where $\tau_{\alpha\alpha\beta\beta}$ is in Hz, G_α are rotational constants, and k_i are the force constants k_s and k_θ. The derivatives $\partial G/\partial R_i$ were calculated numerically and values are given in Table VIII. Using the experimental results for τ_{aaaa}, τ_{bbbb}, and τ_{cccc} with the above model gives $k_s = 0.0272(8)$ mdyn/Å and $k_\theta = 0.0354$ mdyn Å.

The discovery and characterization of the furan-argon complex and the benzene-HCl complex[11] indicates the aromatic π-electron system in ring compounds can act either as a Lewis acid or a Lewis base. This suggests that interactions between π-electron systems of two aromatic ring compounds should be important in the formation of stacked complexes.

Acknowledgment. Equipment was purchased using support from the National Science Foundation. Acknowledgment is made to the donors of the Petroleum Research Fund, administered by the American Chemical Society, for partial support of this research. J. A. Shea was very helpful with spectral assignments in the early phases of this work. Discussions with Peter Beak on synthesis of [2-D]furan and structure of the complex played an important role in the successful completion of this project.

Registry No. Furan-Ar, 84812-22-6; [2-D]furan-Ar, 84812-23-7.

pH Jump: Kinetic Analysis and Determination of the Diffusion-Controlled Rate Constants

Menachem Gutman,*[1] Esther Nachliel, Eli Gershon, Rina Giniger, and Ehud Pines

Contribution from the Department of Biochemistry, Tel-Aviv University, Tel-Aviv 69978, Israel. *Received August 16, 1982*

Abstract: Excitation of proton-emitter compounds such as 8-hydroxypyrene-1,3,6-trisulfonate or sulfonated β-naphthol derivatives by short, intensive laser pulses discharges protons into the solution. These protons are readily detected by their reaction with pH indicators. The kinetics are followed by transient light absorption techniques with a time resolution of 100 ns. The observed proton cycle, protonation and relaxation of the indicator, is a sum of simultaneous first- and second-order reactions between the various reactants. This dynamic is a complex function of all rate constants and reactant concentrations. In the present study, we employed a numerical solution of nonlinear differential rate equations to simulate the dynamics of the observed proton cycle. This analysis permits a direct determination of the diffusion-controlled rate constants of all participating reactions with an accuracy better than 20%.

The laser-induced pH jump[2,3] employs the pH shift of electronically excited aromatic alcohols[4] for rapid acidification of aqueous solutions. Excitation of a proton emitter, such as hydroxypyrenetrisulfonate[5] in dilute solution by a short laser pulse, lowers the pH by 3-4 log units within a few nanoseconds.[3] The protons dissociate from the excited molecules and are detected by their reaction with pH indicator present in the solution.

The proton cycle consists of two sets of temporally resolved reactions: the reactions between the excited molecules and the reactions between the ground-state compounds.

(1) During the 1982-1983 academic year, refer correspondence to M. Gutman, Department of Chemistry, M.I.T., Cambridge, MA 02139.

(2) Gutman, M.; Huppert, D. *J. Biochem. Biophys. Methods* **1979**, *1*, 9-19.

(3) Gutman, M.; Huppert, D.; Pines E. *J. Am. Chem. Soc.* **1981** *103*, 3709-3713.

(4) Forster, Th. *Z. Elektrochem.* **1950**, *54*, 42-46.

(5) Abbreviations: PhOH and PhO^- are the neutral and anionic forms of the proton emitter; HIn and In^-, the protonated and deprotonated forms of the indicator; HPTS, 8-hydroxypyrene-1,3,6-trisulfonate; BCG, bromocresol green.

0002-7863/83/1505-2210$01.50/0

Excited-state reactions are very fast. The proton dissociates during the laser pulse (10 ns fwhm) and the remaining excited anions (PhO^-) decay within the response-time of the electronic system (~30 ns). Thus, the dynamics of the excited state are not observed in this experiment.

At the end of the photodissociation, the equilibrium concentrations of the reactants are displaced, with a significant increase in H^+ and PhO^-. Both In^- and PhO^- compete for the discharged proton; however, since PhO^- is a stronger base, the protonation of In^- will be a transient event. In any case, whenever HIn dissociates, the competition between In^- and PhO^- resumes. Thus, the cyclic event consists of superpositioned first-order and second-order reactions taking place simultaneously.

Because of this complexity, the transformation between the observed, macroscopic rate constant and the rate constants of the partial reactions calls for solution by nonlinear parametric differential equations. The numerical solution is carried systematically by varying the kinetic parameters. Those giving the best fit to the experimental results are taken as the appropriate rate constants of the partial reactions.

As the reaction is unrestricted by the electrical conductivity of the solution, the pH jump is suitable for measuring the effect of the ionic strength on the kinetics of diffusion-controlled reactions between ions. This capacity is exemplified by measuring the rate of proton recombination with two anions over a wide range of ionic strengths (0.0006–0.2 M). The results are in accordance with the theoretical considerations.[6]

Proton transfer between donor and acceptor in water proceeds both through a dissociation–recombination pathway and through proton exchange between the reactants, which takes place during their encounter. The contribution of the direct proton exchange varies with the nature of the reactants. Electrostatic forces and steric hindrance are much more crucial in this mechanism than in the free proton diffusion mechanism.[7] Our method is sensitive enough to follow the kinetics of each pathway under conditions where both systems are operative. The rate constants of these reactions are compared with the rates estimated according to Debye.[8]

Experimental Section

Materials. 8-Hydroxypyrene-1,3,6-trisulfonate, laser grade, was purchased from Kodak. 2-Naphthol-3,6-disulfonate, 2-naphthol-6-sulfonate, and 2-naphthol were Fluka products, twice crystallized before use. Bromcresol green, purchased from Merck, was used without any further purification.

Methods. The proton emitter and the pH indicator were dissolved in bidistilled water. The sample was placed in 1 × 1 cm quartz cuvette and its contents was mixed constantly by a magnetic stirrer. The pH of the solution was adjusted to the desired pH by addition of dilute HCl or NaOH, and continuously monitored during the experiment.

The sample was excited by Molectron UV 14 nitrogen laser pulses (~10 mJ, 10 ns, full width at half-maximum). The focused excitation beam (15 × 3 mm) irradiated the cuvette with an energy density of 0.5–1 MW/cm^2. The probing light beam (HeNe laser), perpendicular to the propagating excitation beam, passed through the excited volume 1 mm behind the front face of the cuvette. Following transmission through the cell, the probe beam was collimated through a 1-mm pinhole at the entrance of an Aminco Bowman monochromator, which was placed 1.5 m away from the cuvette—a point where the fluorescence originating in the cell is significantly decreased.

The signal of the EMI 9684 B photomultiplier was fed into a Biomation 8100 transient recorder and accumulated by a Nicolet 1170 signal averager. The signal processing system was triggered by a IP39 photodiode. The outcoming time-resolved, averaged signals were plotted on an X–Y recorder.

Results

Reaction between Indicator, Proton Emitter, and Protons following a Laser Pulse. The experimental system consists of a pH indicator (In^- and HIn)[5] and a proton emitter (PhOH) dissolved in water at a given pH.[9] A laser pulse is used to excite the proton emitter to its first excited electronic singlet state, which, after a rapid proton dissociation, decays to the ground state with time constant $\tau = 6$ ns. Thus a few nanoseconds after the pulse, the concentration of the dissociated proton emitter (PhO^-) is higher than its equilibrium concentration by an increment defined as X_0.

The discharged proton can combine with the anions (PhO^- and In^-) which are present in the solution. The protons which reacts with the indicator increase HIn concentration by a time-dependent increment (Y) which decays by dissociation and exchange with PhO^- or OH^-.

In our case, the reaction is carried out in a slightly acidic solution (pH <6) and thus the reactions of the HIn and H^+ with OH^- are negligible. Since $HPTS^{4-}$ and the protonated indicator, $BCGH^-$, are negatively charged, they repel each other. Consequently, the probability of any encounter or proton exchange between them is very small.

The reactions which describe the relaxation of the system and the respective time-dependent concentrations of the reactants are given by

$$PhO^- + H^+ \underset{k_2}{\overset{k_1}{\rightleftharpoons}} PhOH \qquad (I)$$

$$In^- + H^+ \underset{k_4}{\overset{k_3}{\rightleftharpoons}} HIn \qquad (II)$$

We defined the concentrations of all the reacting species in terms of their equilibrium concentrations ($\overline{PhO^-}$, $\overline{PhOH}$, $\overline{In^-}$, $\overline{HIn}$, $\overline{H^+}$) and two time-dependent functions, X and Y, such that

$$(PhO^-)_t = \overline{PhO^-} + X \qquad (PhOH)_t = \overline{PhOH} - X$$

$$(In^-)_t = \overline{In^-} - Y \qquad (HIn)_t = \overline{HIn} + Y$$

$$(H^+)_t = \overline{H^+} + X - Y$$

The initial conditions are $X(0) = X_0 = Y(0) = 0$.

The differential rate equations which describe the time dependence of X and Y are

$$\frac{d[PhO^-]}{dt} = \frac{dX}{dt} = (-k_1([H^+] + [\overline{PhO^-}]) - k_2)X + k_1[\overline{PhO^-}]Y - k_1X^2 + k_1XY \qquad (1)$$

$$-\frac{d[In^-]}{dt} = \frac{dY}{dt} = k_3[\overline{In^-}]X - (k_3([\overline{H^+}] + [\overline{In^-}]) - k_4)Y - k_3XY + k_3Y^2 \qquad (2)$$

These equations can be solved either by numerical methods or, after omission of the nonlinear terms (X^2, Y^2, XY), algebraically. In order to delete these terms, the initial conditions must be such that $[PhO^-]$, $[PhOH] \gg X$ and $[In^-]$, $[HIn] \gg Y$. Such initial conditions imply that both emitter and indicator have similar pKs and that the experiment is carried out at a pH close to the pK of the reactants. To avoid such restrictive conditions, we prefer to use a numerical solution for nonlinear equations.[10]

The independent parameters which control the numerical solution are as follows: k_1, k_3, and X_0. The other two rate constants (k_2 and k_4) are already set by the equilibrium constants: $K_{43} = k_4/k_3$; $K_{21} = k_2/k_1$. In order to find the best fit, the two diffusion-controlled rate constants of protonation, k_1 and k_3, are varied in the range of 10^9 to 2×10^{10} M^{-1} s^{-1}.[11-13] The other independent

(6) Lietzke, M.; Stoughton, R. W.; Fuoss, R. M. *Chem. Ber.* **1968**, *59*, 36–45. Robinson, R. A.; Stokes, R. H. "Electrolyte Solutions"; Academic Press: New York, 1955.

(7) Eigen, M.; Kruse, W.; Masass, G.; DeMaeyer, L. *Prog. React. Kinet.* **1964**, *2*, 286–305.

(8) Debye, P. *Trans. Electrochem. Soc.* **1942**, *82*, 265–275.

(9) All excited states have already decayed to the ground state 30 ns after the pulse. Since our kinetic studies are measured at a later time, we have only to consider ground-state molecules.

(10) Subroutine Dverk, The ImSL Library, Vol. 1.

(11) This range represents the values of diffusion-controlled, second-order rate constants between ions in water. The highest values was measured for the protonation of $HPTS^{4-}$; see ref. 12.

(12) Forster, Th.; Volker, S. *Chem. Phys. Lett.* **1975**, *34*, 1–6.

Table I. Association and Dissociation Rate Constants of Protons from the Ground State of Proton Emitters and Indicators

compd	k_{ass}[a]	k_{diss}	pK	I
8-hydroxypyrene-1,3,6-trisulfonate	$(18 \pm 1.5) \times 10^{10}$	3600	7.7	0.0006
2-naphthol-3,6-disulfonate	$(7 \pm 1.5) \times 10^{10}$	45	9.2	0.004
2-naphthol-6-sulfonate	$(7.6 \pm 0.4) \times 10^{10}$	48	9.2	0.002
β-naphthol	$(1 \pm 0.1) \times 10^{10}$	5	9.3	0.001
bromcresol green	$(4.2 \pm 0.1) \times 10^{10}$	4.7×10^5	4.95	0.0006

[a] The values given are the average of 5-7 independent experiments.

Table II. Effect of the Ionic Strength on the Rate Constant of Protonation of 8-Hydroxypyrene-1,3,6-trisulfonate and Bromcresol Green[a]

	8-hydroxypyrene-1,3,6-trisulfonate				bromcresol green				
[NaCl]	$k_{ass} \times 10^{10}$	γ^b	γ^c	γ^d	$k_{ass} \times 10^{10}$	γ^b	γ^c	γ^d	I
-	18 ± 1.5	-	-	-	4.2 ± 0.1	-	-	-	0.0006
0.015	11.5 ± 1.5	0.64	0.76	0.80	3.9 ± 0.1	0.93	0.98	0.92	0.015
0.025	10 ± 1.5	0.56	0.73	0.79	3.8 ± 0.15	0.91	0.93	0.91	0.025
0.05	9 ± 2.0	0.5	0.67	0.76	3.7 ± 0.2	0.87	0.91	0.85	0.050
0.2	7.5 ± 1.5	0.41	0.54	0.69	3.3 ± 0.15	0.79	0.84	0.78	0.20

[a] All experiments were carried out with 100 μM HPTS, 50 μM GCG in the presence of the salt concentrations indicated. [b] This experiment. [c] Calculated according to Davis.[6] [d] Calculated according to Lietzke.[6]

parameter, X_0, is estimated from the initial rate of HIn formation. Within this range of estimated parameters, simulations are systematically iterated until a set of parameters (k_1, k_3, X_0) is found which yields the best curve fitted to the experimental one.

Figure 1 depicts such a typical simulation. The initial velocity of the reaction led to an estimate for X_0 of 4–5.5 μM, and within this range of X_0 we varied both k_1 and k_3. Figure 1A depicts simulations with $k_1 = 1.8 \times 10^{11}$ M^{-1} s^{-1} and three values of k_3 ($(3, 4.2, 5) \times 10^{10}$ M^{-1} s^{-1}). In Figure 1B, k_3 was kept constant (4.2×10^{10} M^{-1} s^{-1}) and k_1 was varied ($(1.6, 1.8, 2.2) \times 10^{10}$ M^{-1} s^{-1}). In both figures, $X_0 = 4.25$ μM was used. The fit could not be improved further by any change of X_0. Thus we conclude that $k_1 = (1.8 \pm 0.2) \times 10^{11}$ M^{-1} s^{-1} [3,12] and $k_3 = (4.2 \pm 0.5) \times 10^{10}$ M^{-1} s^{-1}.[3]

Figure 1C represents the simulated functions of the reactants HIn, PhO^-, and H^+. It is of interest to note that the H^+ concentration decays very rapidly to its prepulse level ($\tau < 0.5$ μs)[3] whereas, as pointed out before,[13] the perturbed state of the indicator and PhO^- linger for a much longer time.

We measured the dynamics of the proton cycle of other proton emitters by using bromcresol green as the indicator. The rate constants of proton association and dissociation are listed in Table I.

Correlation between the Reaction Rate Constants and the Macroscopic Parameters of the Reaction. The superpositioning of the simulated curve over the experimental one can detect even minor deviation between the lines, but it is inconvenient for quantitative comparison of the results. Thus, we characterized the curves by four macroscopic parameters: T_{max} and Y_{max}, the time and concentration coordinates of the maximum, two rate constants of signal built up (γ_1) and decay (γ_2). None of these reactions is a true exponential function but both can be so approximated over a certain range of their dynamics (60% of built up and 60% of initial signal decay). These macroscopic parameters were calculated by the same algorithms, using the experimental results and the simulated functions. The comparison of the experimental parameters with the simulated ones is convenient for esimation of the rate constants, as exemplified in Figure 2. The variation of each of the macroscopic parameters is drawn for three k_3 values ($(3.2, 4.2, 6.2) \times 10^{10}$ M^{-1} s^{-1}) while k_1 varies from 1 to 25×10^{10} M^{-1} s^{-1}. The accepted values of k_1 and k_3 are those which generate correctly the four measured macroscopic parameters. The experimental macroscopic parameters of the curve of Figure 1 will lead to coherent values of k_1, provided that $k_3 = 4.2 \times 10^{10}$ M^{-1} s^{-1}.

Effect of Initial Conditions on the Dynamics of the Proton Cycle. The most dominating process during the proton cycle is the competition between PhO^- and In^- for the protons. Thus the prepulse concentration of these reactants will determine the shape and duration of the measured event. The variation of the measured macroscopic paremeters with the prepulse pH, and the computed function are drawn in Figure 3.

The effect of PhO^- concentration on γ_1 and γ_2 is given in Figure 4A,B. Increasing the competivity of PhO^- for H^+ enlarges both γ_1 and γ_2. T_{max} is shortened and the amount of HIn formed diminishes (not shown). It is of interest to note that above certain concentrations of PhO^-, γ_2 remains constant. This is the limiiting case where PhO^- competes successfully for any proton dissociationg from HIn, consequently the rate-limiting step of the reaction becomes k_4. If the proton cycle can be measured under conditions where $[PhO^-] > [In^-]$, then γ_2 can be accurately equated with k_4.

The effect of $[In^-]$ is given in Figure 4B. As expected, there is hardly any effect on γ_2, whereas γ_1 increases nearly linearly. Once $[\overline{In^-}] \gg ([\overline{PhO^-}] + X)$, the formation of HIn becomes effectively a pseudo-first-order reaction and γ_1 will become a linear function of $[In^-]$, with a slope of k_3.

Effect of the Proton Pulse Size on the Macroscopic Parameters. X_0, the parameter of the pulse size, depends linearly on the energy density of the excitation beam[3] and the emitter concentration. As a result, the pulse size may very between successive experiments. In order to estimate the effect of this variance on the macroscopic parameters, we simulated a set of experiments where the pulse size was varied systematically from X_0 to 1 to 40 μM (Figure 5).

The protons are produced together with their conjugate bases and the prepulse pH is regained very rapidly (Figure 1C). Consequently, the effect of the pulse size is not similar to the effect of increasing the prepulse concentration of the other reactants, $\overline{PhO^-}$ or $[\overline{In^-}]$.

Y_{max} increases steeply with X_0. However, at high X_0 values the line curves, reflecting the higher probability of an encounter between H^+ and PhO^-. T_{max} is less sensitivie to X_0, while the two rate constants, γ_1 and γ_2, are nearly independent of the pulse size (not shown).

Effect of Ionic Strength on the Rate Constants of Protonation of PhO^- and In^-. Rapid kinetics using the electric field jump are limited to solutions with very low electric conductivity. The temperature jump calls for solutions with high conductivity. The pH jump can operate irrespective of the electric conductivity. Thus, the same method can be used over a wide range of ionic strengths, up to very concentrated salt solutions.[14,15]

(13) Gutman, M.; Huppert, D.; Pines, E.; Nachliel, E. *Biochim. Biophys. Acta* **1981**, *642*, 15-26.

(14) Gutman, M.; Huppert, D.; Nachliel, E. *Eur. J. Biochem.* **1982**, *121*, 637-642.

(15) Huppert, D.; Pines, E.; Gutman, M.; Nachliel, E. *J. Am. Chem. Soc.*, in press.

(16) Eigen, M. *Argew. Chem.* **1964**, *3*, 1-19.

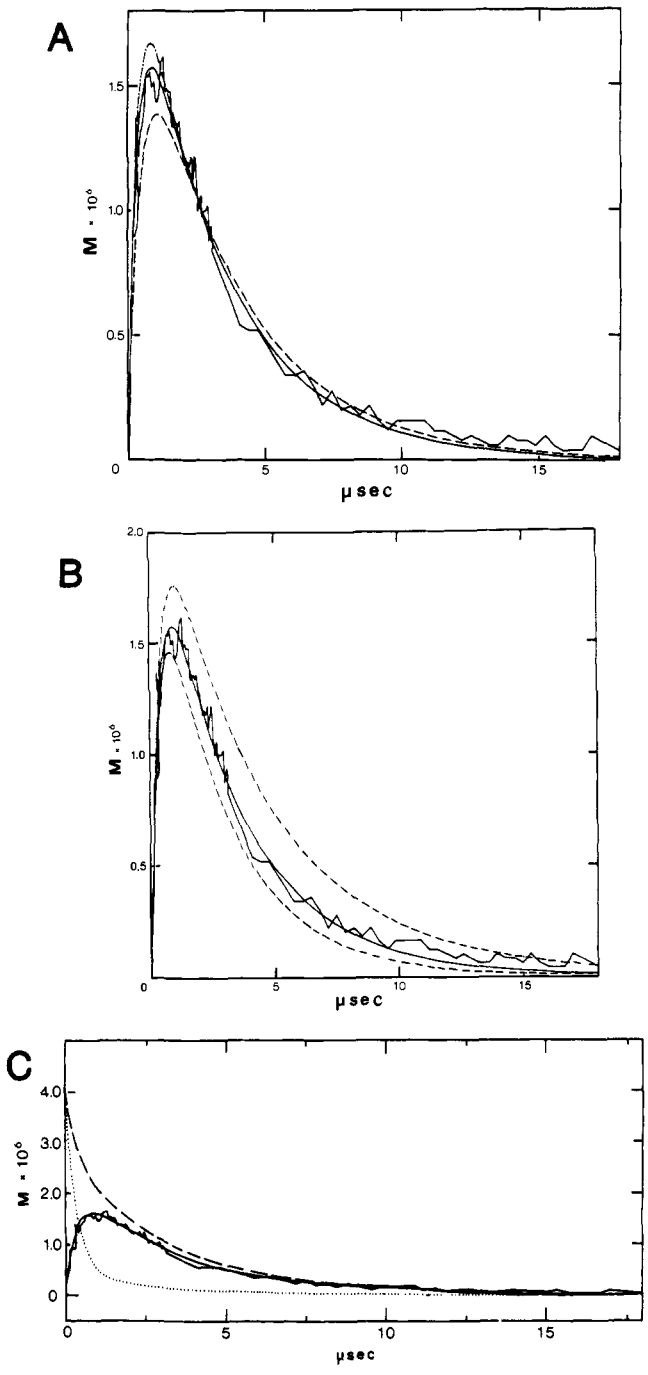

Figure 1. Experimental results and simulated curves of the proton cycle. The experiment was carried out in the presence of 40 μM bromcresol green, 100 μM 8-hydroxypyrene-1,3,6-trisulfonate, pH 5.88, room temperature. 50 readings of the experimental curve, in the range of 0–3.3 μs, at 68-ns intervals, and 50 readings in the range of 1.0–17.7 μs at 340-ns intervals are drawn, together with the values of the simulated curve, calculated for the same time points. (A) The simulated reactions were computed for the following parameters: $k_1 = 18 \times 10^{10}$ M^{-1} s^{-1}; $X_0 = 4.25$ μM; $k_3 = 3.2 \times 10^{10}$ (--), 4.2×10^{10} (–), $5.2 \cdot 10^{10}$ (-·) M^{-1} s^{-1}. After ~5 μs the lines for 4.2 and 5.2×10^{10} M^{-1} s^{-1} practically overlap. (B) The simulated reactions were computed for the following parameters: $k_3 = 4.2 \times 10^{10}$ M^{-1} s^{-1}; $X_0 = 4.25$ μM; $k_1 = 16 \times 10^{10}$ (---), 18×10^{10} (–), 22×10^{10} (---) M^{-1} s^{-1}. (C) Simulation of the variation with time of $(PhO^-)_t$ (---); $(HIn)_t$ (–); and $(H^+)_t$. The experimental values of $(HIn)_t$ are also drawn. $k_1 = 18 \times 10^{10}$ M^{-1} s^{-1}; $X_0 = 4.25$ μM; $k_3 = 4.2 \times 10^{10}$ m^{-1} s^{-1}.

The reactions of $HPTS^{4-}$ and BCG^{2-} with H^+ are diffusion-controlled reactions between charged particles and thus are modulated by the ionic strength.[7,8,16] We measured the dependence of the rate constants of these reactions on the ionic strength over a wide range of NaCl concentrations (I = 0.006–0.2 M). The experiment illustrated in Figure 1 was repeated in the salt solutions listed in Table II, and the rate constants, k_1 and k_3, were calculated by the simulation technique. The activities of $HPTS^{4-}$ and BCG^{2-}, derived from the measured rate constants, are compared with the calculated values.[6]

Detection of Direct Proton Exchange between the Reactants. The intensive electrostatic repulsion between the pyrenetrisulfonate anion (Z = 4) and the protonated indicator ($BCGH^-$) lowers the probability of their encounter by a 100-fold.[7,8,12] Thus a direct proton exchange between these two reactants

$$HIn + PhO^- \underset{k_6}{\overset{k_5}{\rightleftharpoons}} In^- + PhOH \qquad (III)$$

is slowed both by slow diffusion ($D = 2–3 \times 10^{-6}$ cm^2 s^{-1}) and electric repulsion.

In order to evaluate whether our experimental system can detect the contribution of a direct reaction, we substituted the highly charged emitter, $HPTS^{-3}$, with the neutral emitter, β-naphthol. The protonation cycle of bromcresol green, in the presence of β-naphthol, is depicted in Figure 6. Calculations which did not account for the contribution of the direct proton exchange (reaction III) gave unsatisfactory simulations. However, including the rate constants of reaction III in the differential rate equations led to the simulation seen in Figure 7.

The rate constant of the spontaneous direction of the proton exchange $k_5 = 5 \times 10^4$ M^{-1} s^{-1} is compatible with the value estimated according to Debye and the viscosity of the solution.

The reaction between PhO^- and HIn can be further augmented by carrying the experiment at pH $\ll$ pK_{43}. Under those conditions the increment of HIn by OH dissociation will be very small but the bimolecular reaction between the formed PhO^- and HIn will be fast. At proper conditions the net changes in HIn might be negative, i.e., a transient deprotonation.

A very short time after the pulse, Y can be assumed to be zero. Thus, the time derivative of Y can be either positive or negative, depending on the Y term of the differential rate equation of Y which includes the rate constant of reaction III:

$$\frac{dY}{dt} = [k_3(\overline{In^-}) - k_6(\overline{In^-}) - k_5(\overline{HIn})]X \qquad (3)$$

The transition from HIn formation (by reaction with H^+) to HIn consumption (by proton exchange with the increment of PhO^-) will take place at a certain ratio of $[InH]/[In^-]$:

$$\left(\frac{[HIn]}{[In^-]}\right)_0 = \frac{k_3}{k_5} - \frac{K_{21}}{K_{43}} \qquad (4)$$

For each pair of indicator–proton emitter, there will be a point, pH′, where the response of the indicator will shift its direction. At higher pH values, the indicator will be acidified, while at lower pH values alkalinization will dominate. The value of this transition is given by

$$pH' = pK_{43} - \log\left(\frac{[HIn]}{[In^-]}\right) = pK_{43} - \log\left[\frac{k_3}{k_5} - \frac{K_{21}}{K_{43}}\right] \qquad (5)$$

Once $(k_3/k_5) \gg (K_{21}/K_{43})$, we can approximate this by

$$pH' = pK_{43} - \log\frac{k_3}{k_5} \qquad (6)$$

At the pH below pH′, the reaction with the conjugated base dominates. pH′ differs from the pK by log (k_3/k_5)—the ratio of the rates of In^- protonation (k_3) and HIn reaction with a conjugated base (k_5).

The effect of the initial pH on the direction of HIn response is demonstrated in Figure 7A,B. At pH 7.1, the bromcresol purple (pK = 6.3) is protonated; at a lower pH (5.12), it gets deprotonated by the reaction with the β-naphtolate formed by the pulse.

Discussion

The laser-induced pH jump enables an accurate measurement of diffusion-controlled rate constants of the reactions between

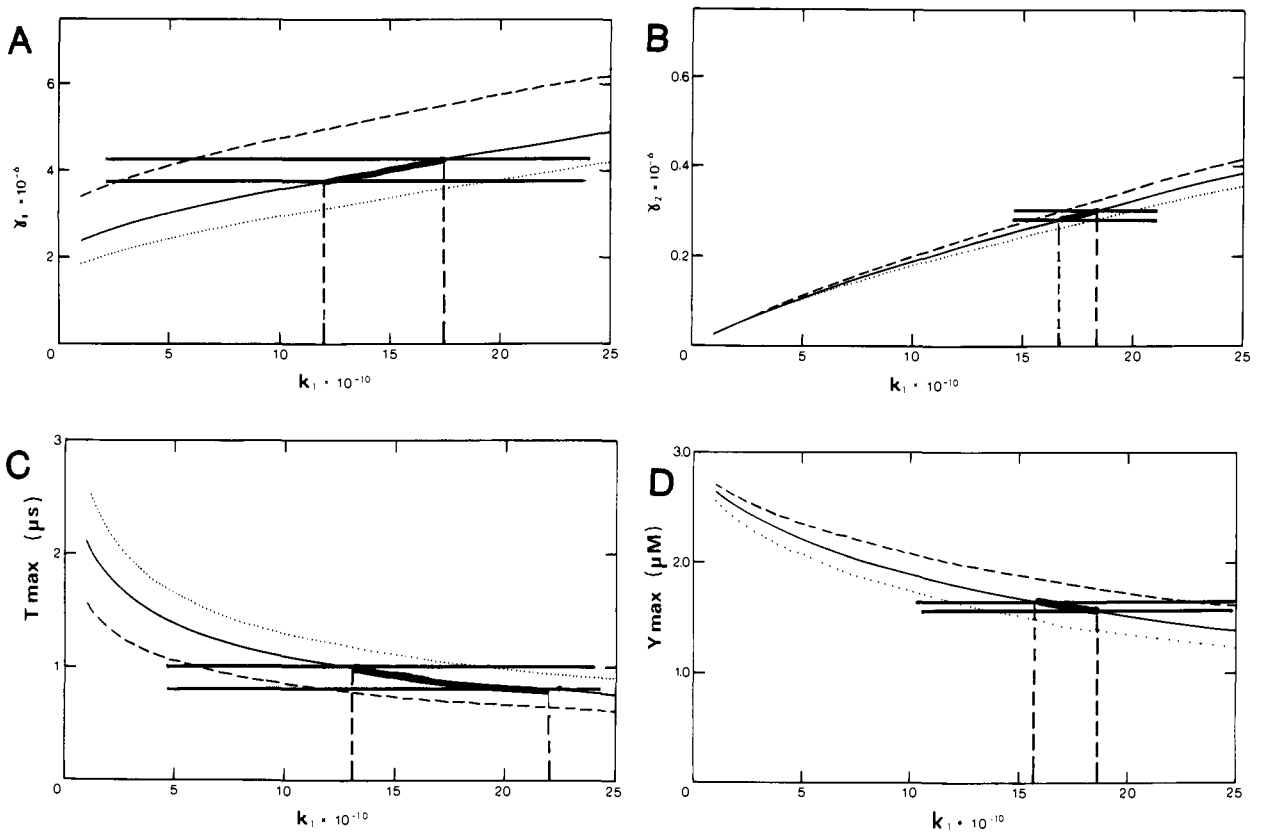

Figure 2. Dependence of the macroscpic parameters on the rate constants. The macroscopic parameters were calculated for simulations describing the experimental conditions defined in Figure 1. The lines represent γ_1 (A), γ_2 (B), T_{max} (C), and Y_{max} (D) as a function of the rate of protonation of PhO^-. In each figure there are three curves calculated for k_3 with the values of 3.2×10^{10} M^{-1} s^{-1} (···), 4.2×10^{10} M^{-1} s^{-1} (–) and 6.2×10^{10} M^{-1} s^{-1} (---) The experimentally determined macroscopic pararameters are indicated as parallel lines, their separation being the width of the experimental accuracy.

protons and specific acceptors. It has the advantage of good time resolution and simple methodology, and it is not hampered by high salt concentrations present in the system. The pH jump technique can be applied equally for measuring the rate constants of protonation of both small molecules and macromolecular structures.[13]

The rate constant of a diffusion-controlled second-order reaction is a function of the physical properties of both the reacting molecules and the solvent.[8] Its magnitude depends on the radii of the reacting species, their diffusion coefficients, their electrostatic potential at the reaction distance,[7] and the steric factor (σ) which furnishes an independent method for evaluation of the geometry of the reactants.[17] Solvent properties affecting reaction rates include viscosity, dielectric constant, and ionic screening. In the case where one of the reactants is a proton, the rate constant is sensitive to all mechanisms which affect the abnormal diffusion coefficient on H^+ in protoic solvents.[18]

As demonstrated in this manuscript, the combination of the pH jump technique and numerical analysis can produce accurate measurements of the rate constants (Table I). The simulation technique can fit a theoretical curve within the boundaries set by the electronic noise (Figure 1) and, with respected experiments, an accuracy of better than 20% can be obtained.

With the instrumentation described above, we found it convenient to limit the indicator concentration ($\epsilon \sim 3 \times 10^4$ M^{-1} cm^{-1}) to absorbance range of 0.2–3 A cm. At lower concentrations of indicator the dilution flattens to the signal and makes it poorly resolved. The rise time becomes shorter, the decay is faster, and the signal diminishes in size (Figure 4B).

The upper limit of indicator concentration is limited by the fluorescence of the proton emitter. It should be remembered that of the 1 MW of excitation energy ~10–100 KW are irradiated as fluorescence. Unless this emission is reduced at the entrance slit of the photomultiplier below saturation energy of the photomultiplier, nonlinear response are expected. On the other hand, the transient intensity of the probing beam must be big enough to be recorded. Thus a combination of intensive monitoring beam and selective damping of the fluorescence is always needed. Once the absorbance of the monitoring beam increases, more light should be introduced to the monochromator with consequent admission of more fluorescence.

The concentration of the emitter can also vary within a certain range. At low concentration the perturbation is small while at high concentration all of the excitation energy may be adsorbed at the first few millimeters of the solution. Under these conditions the size of the perturbation is highly dependent in the distance of the probed space from the front surface of the cuvette. As pointed out in Figure 5, the magnitude of X_0 has a marked effect on all macroscopic parameters. This may introduce an apparent irreproducibility with every minor change of the monitoring beam's location. Finally, a possible source for error is the accumulation of photoproducts.[19] At an energy density of less than 1 MW/cm^2, no deviations due to photoproducts were observed.[3] Still whenever many events are accumulated over a long time period 3–30 mL of irradiated solution and proper mixing are recommended.

The dynamics most accurately measured is the decay of the signal, γ_2. The relaxation is slow enough to be conveniently measured by currently available instruments. The signal relaxation is a complex function. The initial phase is accurately described by a single exponent, but as it proceeds, the relaxation shows into a long tail. (Some of the tail might even be attributed to stable photo products.[19]) Most of the data, characterized by high signal

(17) Eigen, M.; Hammes, G. G. *J. Am. Chem. Soc.* **1960**, *82*, 5951–5952.
(18) Conway, B. E.; Bockris, J. O'M.; Linton, H. *J. Chem. Phys.* **1956**, *24*, 834–839.
(19) Klaning, V. K.; Goldschmidt, R.; Ottolenghi, M.; Stein, G. *J. Chem. Phys.* **1973**, *59*, 1753–1759. Lachish, V.; Ottolenghi, M.; Stein, G. *Chem. Phys. Lett.* **1977**, *48*, 402–406.

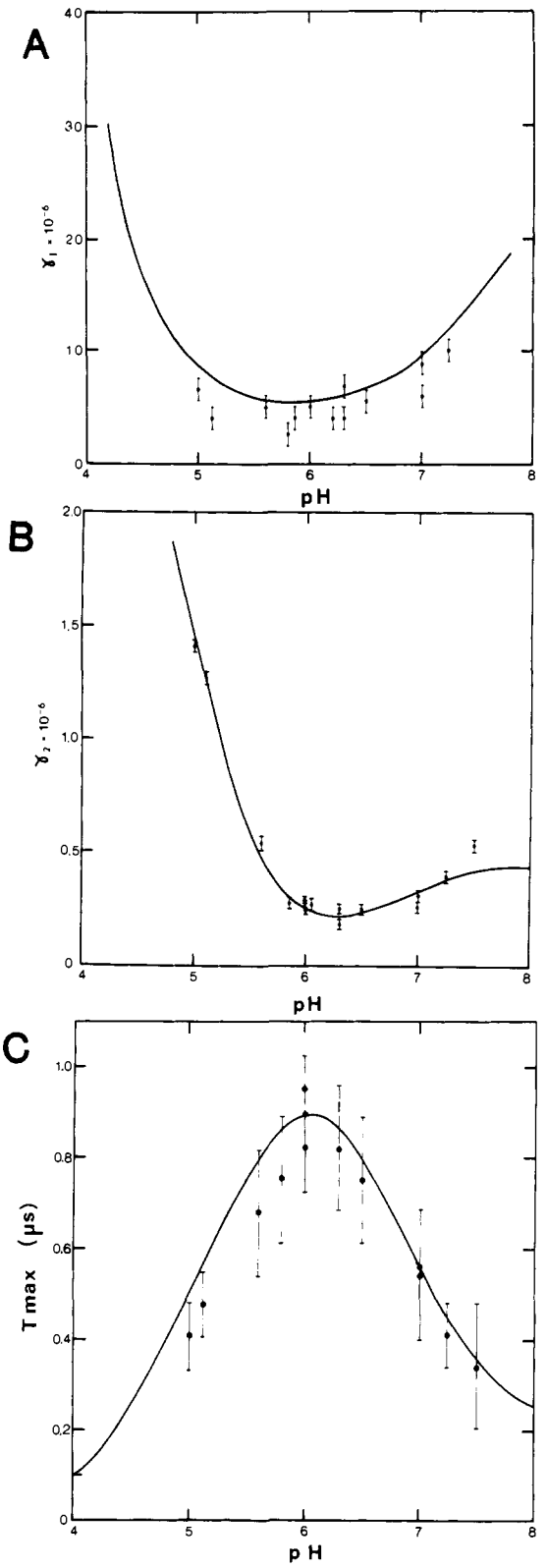

Figure 3. Effect of the initial pH on the macroscopic parameters. The simulations were carried out over the entire pH range indicated and the macroscopic parameters of the calculated line are drawn. The simulated reaction is that given in Figure 1 with the rate constants listed in Table I (X_0 and 4.25 μM). (A) γ_1 vs. pH. (b) γ_2 vs. pH. (C) T_{max} vs. pH. The experimental results are indicated with their error bars.

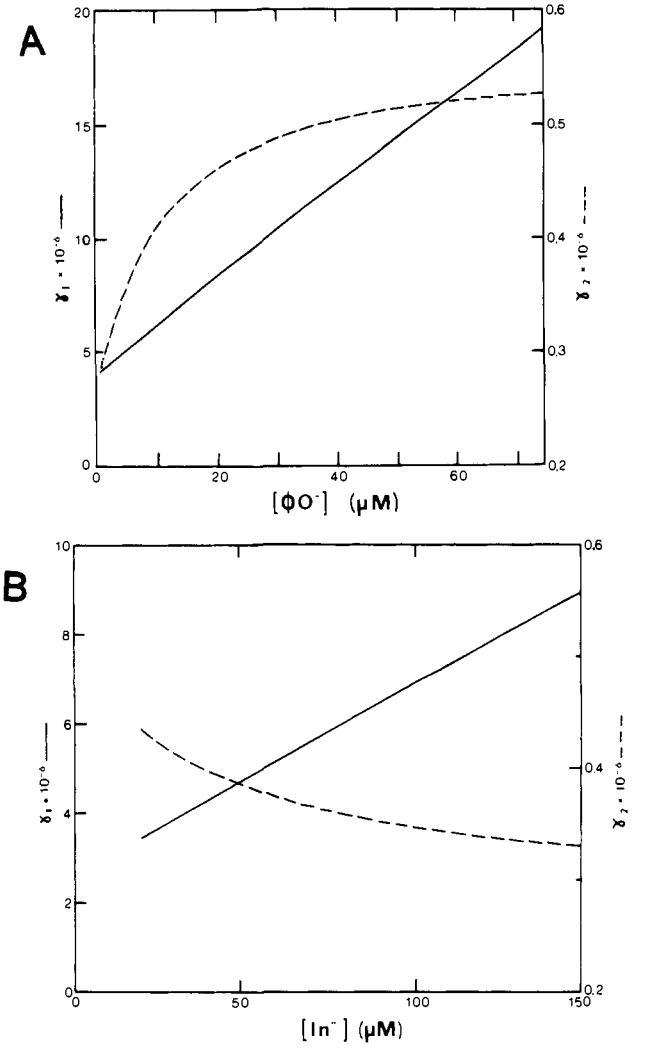

Figure 4. Dependence of the macroscopic parameters on PhO^- concentration (A) and the indicator concentration (B). The experimental conditions, except for indicator concentrations, are defined in Figure 1. The rate constants for 8-hydroxypyrene-1,3,6-trisulfonate and bromcresol green are listed in Table I. X_0 = 4.25 μM.

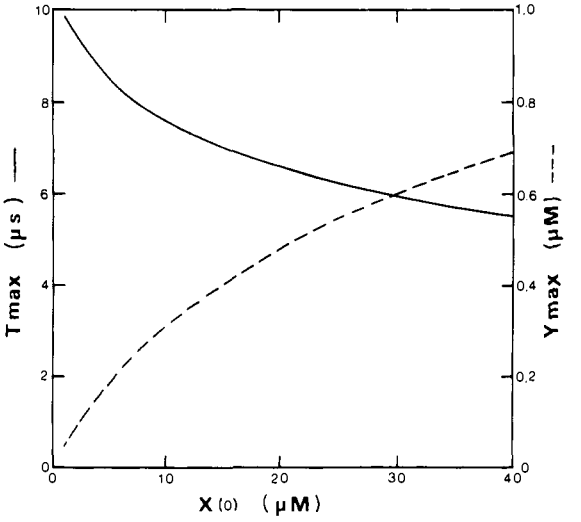

Figure 5. Dependence of the macroscopic parameters on the pulse size (X_0). The experimental conditions are defined in Figure 1. The rate constants are listed in Table I. The pulse size, X_0, was varied between 1 and 40 μM.

to noise ratio, is clustered in the nearly exponential decay curve and is fairly well represented by γ_2. In most cases, γ_2 can be measured with ±10% error.

The rate constant of signal rise, γ_1, is less accurately determined. This signal is built up quickly, reaching its maximum in a few microseconds or less. Thus the ascending section of the curve is limited in resolution: its initial part has an exponential rise but a poor signal to noise ratio due to the small signal size. Fur-

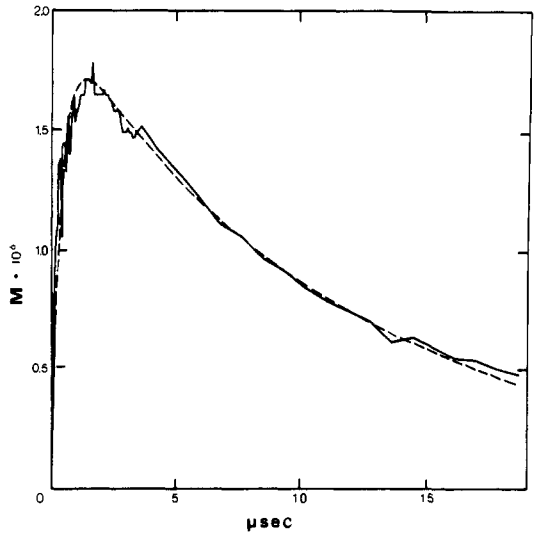

Figure 6. Experimental results and simulated curve for the proton cycle measured with β-naphthol (1 mM), and bromcresol green (40 μM), pH 7.3. The rate constants for bromcresol green are taken from Table I. The simulation curve given in the figure (- - -) corresponds with $k_1 = 1.5 \times 10^{10}$ M^{-1} s^{-1}, $k_5 = 5 \times 10^9$ M^{-1} s^{-1}, $X_0 = 2.7$ μM.

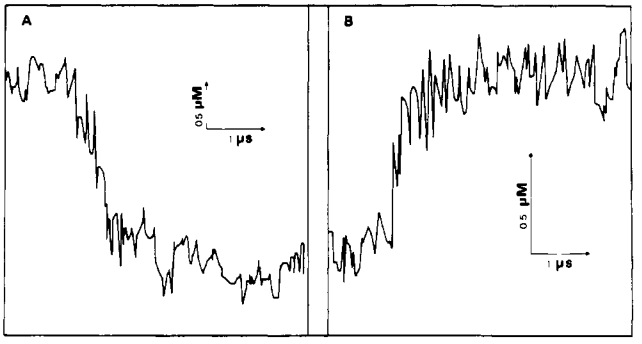

Figure 7. Effect of pH on the response of bromcresol purple during the proton pulse. The reaction mixture contained bromcresol purple 100 μM and β-naphthol 1 mm at pH 7.05 (A) and 5.12 (B). Each tracing is an average of 4096 events. Downward deflection corresponds with protonation of indicator.

thermore, once the measured values become higher, the curve begins to deviate from the exponential function and the data become unsuitable for calculating γ_1. For these reasons, the value of γ_1 is less accurate than that of γ_2. In some experiments, the error might be as high as 30%.

T_{max}, the time when the signal reaches its maximal height, has its own uncertainty due to the flatness of the curve at its maximum and the electronic noise. In the case of a sharply rising, steeply decaying signal, T_{max} can be estimated with an error of ±70 ns. On the other hand, slowly decaying signals have undefined maxima and inaccuracy may be as high as ±1 μs.

The value of Y_{max} for a given experiment can be measured very accurately, with an error of less than 5%. Thus for the purpose of simulation, the amplitude is a very accurate parameter. However, as demonstrated in Figure 7, Y_{max} is highly dependent on X_0, which is a function of the excitation laser output, pulse beam dimensions, observation cell, and monitoring beam geometries. The other parameters are much less affected by the size of this perturbation. Thus, the amplitude is a parameter which may vary quite independently of the rate parameters, γ_1 and γ_2. Therefore, despite the fact that Y_{max} can be an informative parameter for a given experiment, it is unsuited for comparison between different experiments. For these reasons, we did not compare the Y_{max} values among the experiments.

Even though each of the experimental macroscopic parameters bear its own inaccuracy, the combination of the four leads to unambiguous determinations of the reaction rate constants (Figure 2). Table I lists the means of 5–7 independent measurements, carried out under different initial conditions. The results are all reproducable within 20%.

In any chemical system, even with the minimal number of reactants (proton emitter, proton detector and solvent), the number of reactions can be large. In our system, the reactions between H^+ and OH^-, OH^- and HIn, or HIn and PhO^- cannot be ignored a priori. Therefore, in order to simplify the analysis, initial conditions should be selected to minimize the number of possible reactions. Once this precaution is taken and some of the rate constants are known, a more complex system can be methodically analyzed, as illustrated in Figures 6 and 7 (A, B). Figure 6 represents a simulation where the direct proton exchange has been incorporated into the differential rate equations, but a true demonstration of the contribution of this reaction is given in Figure 7 (A, B).

Under certain conditions, the formation of the conjugated base can lead to transient deprotonation of HIn. These conditions have been derived from eq 4 and are defined by eq 5–8. It should be pointed out that the alkalinization of bromcresol purple at pH 5.12 cannot be explained by the formalism of eq 1 and 2. A detailed dynamic analysis with simulative computations will be published separately.

The ratio between the measured rate constants and the values calculated according to Debye's equation is an estimation of the steric factor σ. In the case of the direct proton exchange (reaction III), the measured rate constant ($k_5 = 5 \times 10^9$ M^{-1} s^{-1}) is slightly higher than the rate of encounter between two negatively charged reactants ($BCGH^-$ and β-naphtholate) with $\sum D \sim 5 \times 10^{-6}$ cm^2 s^{-1} and an encounter radius of ~10 Å. Thus for this reaction, $\sigma \sim 1$. In the case of the protonation of β-naphtholate, the rate ($k_1 = 1.5 \times 10^{10}$ M^{-1} s^{-1}, Table I) is ~30% of that estimated by Weller[20] (5×10^{10} M^{-1} s^{-1}). The steric factor σ appearing in Debye's equation is a complex function representing not only the geometry of the reacting molecules, i.e., the fraction of the reacting surface and axis ratio for nonspheric molecules, but also the rate of rotation of the reactants.[21,22,23] A fast rotation of the reactants increases the probability of reaction, but this event must take place before the encounter complex separates. Thus while fast rotational diffusion increases σ, a fast translational diffusion lowers σ.[23] Consequently, the proton exchange between the large rapidly rotating slow-diffusing molecules β-naphtholate and protonated bromocresol green has a higher steric factor than the reaction between β-naphtholate and a free proton. The steric factor estimated for the latter reaction $\sigma \sim 0.3$ is comparable with the surface fraction of the hydroxyl on the β-naphthol,[24] indicating that in this reaction the rotational diffusion is too slow to affect the outcome of the collision.

Acknowledgment. This research was supported by the American Israeli Binational Science Foundation (3101/82).

Registry No. 8-Hydroxypyrene-1,3,6-trisulfonate, 27928-00-3; 2-naphthol-3,6-disulfonate, 148-75-4; 2-naphthol-6-sulfonate, 93-01-6; β-naphthol, 135-19-3; bromcresol green, 76-60-8; bromcresol purple, 115-40-2.

(20) Weller, A. *Z. Phys. Chem. (Wiesbaden)* **1958**, *17*, 224.
(21) Solc, R.; Stockmayer, W. H. *Int. J. Chem. Kinet.* **1973**, *5*, 733–752.
(22) Ricter, P. H.; Eigen, M. *Biophys. Chem.* **1974**, *2*, 255–263.
(23) Shoup, D.; Lipari, G.; Szabo, A. *Biophys. J.* **1981**, *36*, 697–714.
(24) Bondi, A. *J. Phys. Chem.* **1964**, *68*, 441–451.